JACS
JOURNAL OF THE AMERICAN CHEMICAL SOCIETY
Article
pubs.acs.org/JACS

Twinning of Rhombic Colloidal Crystals

Kun Zhao[†,‡] and Thomas G. Mason*[,†,‡,§]

[†]Department of Chemistry and Biochemistry, [‡]Department of Physics and Astronomy, and [§]California NanoSystems Institute, University of California-Los Angeles, Los Angeles, California 90095, United States

Supporting Information

ABSTRACT: We observe twinning of two-dimensional (2D) rhombic colloidal crystals of hard Brownian rhombic platelets. By contrast to square particles, which have higher symmetry but can also form rhombic lattices at high densities, each rhombic particle has a distinguishable bidirectional pointing axis. This key feature, which is not readily seen in rhombic crystals of square colloids, facilitates observations of different types of twinning: contact, polysynthetic, and cyclic. Moreover, we find that the twinned crystals are slightly offset spatially along their shared mirror line. In addition, the average pointing axis of the particles in a single crystal is also offset on average by a small angle, either clockwise or counterclockwise, from the average pointing axis of the rhombic lattice yielding a form of nonlocal chiral symmetry breaking. Because mirror lines between contact twins introduce only a small reduction in the total number of accessible states, compared to a perfect single crystal, twinning and piecewise linear defects are commonly observed. Thus, twinning, which is usually associated with complex compositions in certain minerals, also emerges in a simpler 2D system of entropically driven, hard, achiral objects.

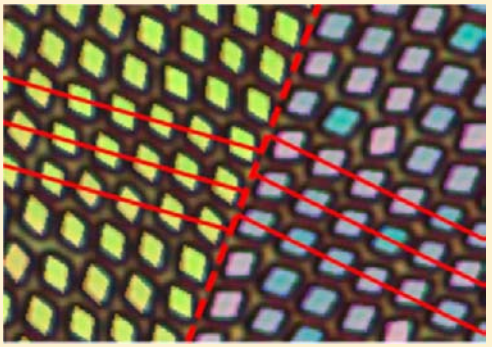

INTRODUCTION

Twinning is commonly found in many different types of crystalline minerals made of atomic or molecular constituents.[1−4] Twinning naturally occurs when lattice points in one crystal are shared as lattice points in another crystal that has a distinguishably different orientation. Twinning is typically classified in several ways, whether based on symmetry of observed structures or on formation processes. The simplest structural twin is the contact twin, in which there is reflection symmetry of the two twinned crystals across a contact plane, also called a mirror plane. Twinned crystals are often beautiful mineral structures, and pyrite (iron disulfide), also known as "fool's gold", commonly exhibits twinning.[5] Twinning can even occur in protein crystals.[6] Twinning has also been observed in three-dimensional (3D) dense systems of colloidal objects that have hard or charge-repulsive interactions.[7−10] However, to date, twinning has not yet been experimentally demonstrated in 2D Brownian systems of hard colloidal objects, including nonspherical colloids that have exotic shapes.[11,12]

Colloidal crystals of hard spheres[13] serve as a basic starting point for examining the origin of atomic and molecular crystals because the spheres have a simple interaction potential, exhibit Brownian motion, and can be observed readily using real-space microscopy,[14] and their trajectories can be directly obtained via video particle tracking.[13,15,16] Often, differently oriented crystalline grains of a colloidal crystal meet at grain boundaries: regions that exhibit an increased amount of disorder. Compared to grain boundaries between single crystals which are commonly observed,[15] twinning in systems of colloidal hard spheres has been reported experimentally only under shear[7] or during seed structure-initiated crystal growth.[10] Beyond spheres, other new colloidal shapes have been synthesized, both using bottom-up[11,12,17] and top-down methods.[18−25] Although crystal twinning has not yet been observed for a limited range of nonspherical shapes examined so far, it is possible that certain shapes could have a greater propensity to form twinned crystal structures.

Recently, a general method of exploiting roughness-controlled depletion attractions (RCDA) of custom-shaped microscale lithographic platelets has been developed, permitting the study of two-dimensional (2D) Brownian systems of hard microscale particles that are ideal for simple optical microscopy.[26,27] The classic depletion attraction arises entirely from entropic considerations of hard colloidal objects and occurs when larger colloids are mixed with smaller nanoscale colloids, known as depletion agents,[28] in a colloidal dispersion. As both the larger and the smaller colloids diffuse in the liquid, the smaller colloids diffuse more rapidly and effectively exert an osmotic pressure on the surfaces of the larger ones. When two larger colloids diffuse into close proximity with one another, the smaller colloids become excluded from the region in between the larger ones, thereby creating an attractive force between the larger colloids due to an imbalance in the osmotic pressure acting over their surfaces.[26] The classic depletion attraction is very short in range, corresponding to the diameter of the depletion agent and can be highly sensitive to the shape and size of the larger colloids relative to the smaller colloids. Beyond the classic case, RCDA alters the strength and anisotropy of the depletion attraction by tuning the size of a

Received: August 18, 2012
Published: October 18, 2012

dx.doi.org/10.1021/ja308214m | J. Am. Chem. Soc. 2012, 134, 18125−18131

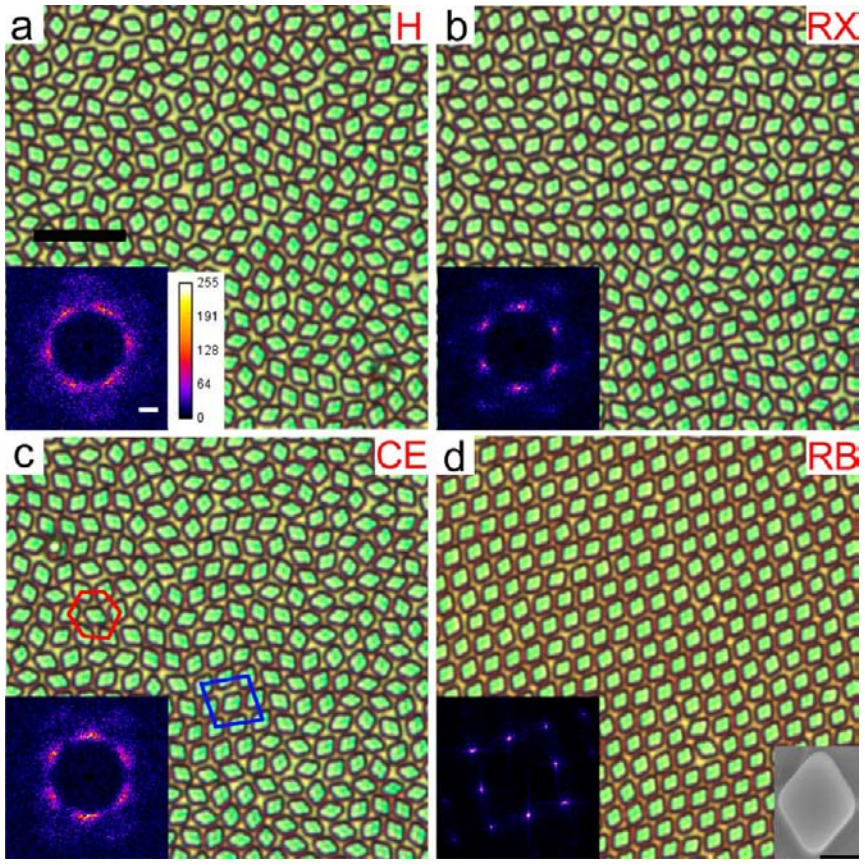

Figure 1. Transmission optical micrographs of Brownian rhombs at particle area fractions ϕ_A: (a) 0.56, hexatic (H); (b) 0.57, RX crystal, (c) 0.59, CE; and (d) 0.62, RB crystal (scale bar = 10 μm). Insets, lower left corners: FFT intensities calculated from real-space images (white scale bar = 0.2 μm^{-1}). Nearest neighbors around a central particle in (c): RX (red hexagon) and RB (blue rhombus) crystallites. A single point defect (orthogonal orientation) of a rhomb particle can be seen in the lower middle region of the RB crystal in (d). Inset in the lower right corner of (d): scanning electron micrograph of a rhombus particle (small black scale bar = 1 μm).

nanoscale depletion agent relative to the nanoscale roughness on the larger colloids. The roughness on specific surfaces of the larger colloids can be made to be larger or smaller than that of the depletion agent; typically, the surfaces with higher roughness do not strongly attract even when surfaces having smaller roughness do attract. For custom-shaped larger colloids made lithographically, the edges of the particles are typically rougher than their faces. So, by introducing a spherical depletion agent at an appropriate concentration having a diameter in between the two roughness length scales, we create a system in which the effective in-plane attraction between two edges of platelets is less than thermal energy k_BT, yet the depletion attraction between the faces of platelets and the flat wall of container is high enough to hold the platelets parallel to the wall to form a lubricated monolayer in which the platelets can still diffuse (see ref 20, Supplemental Material). Thus, for the 2D system, in-plane particle interactions between the edges of the platelets are effectively hard. The volume fraction of platelets is dilute enough that the platelets settle and their faces become attracted to the lower wall of the microcuvette before aggregates of platelets form in the bulk.

Using RCDA, several different systems of hard regular polygons, such as pentagons,[20] squares,[25] and triangles,[21] in 2D have revealed a rich variety of phases and quenched disordered structures. In these systems, Brownian fluctuations are very important, and entropy maximization effectively governs the phase behavior. Even in these rich systems of highly symmetric polygons, the effect of twinning has not been observed. Evidently, obtaining robust manifestations of twinning in 2D Brownian colloidal systems of a single type of monodisperse hard shape requires geometrical features of particle shape that have not yet been sampled in prior studies.

Here, we report and explain observations of twinning in 2D rhombic (RB) Brownian colloidal crystals composed of hard, monodisperse, rhombic platelets (i.e. rhombs, internal angle 72°, edge length $L = 2.0 \pm 0.1$ μm, and thickness $h = 2.0 \pm 0.1$ μm) made using optical lithography (see Supporting Information). Although rhombs are achiral and have a single edge length L, similar to squares, rhombs additionally have unequal internal angles, which reduces the four-fold rotational symmetry of squares to two-fold for rhombs. Thus, a rhomb has a uniaxial (i.e., headless) director[29,30] along its long diagonal. We show that, while rhombs having a 72° internal angle exhibit a qualitatively similar phase behavior as squares when the particle area fraction ϕ_A is increased to higher densities, by contrast to squares, rhombs have a propensity to readily exhibit twinning in a RB crystal phase. The twinned RB crystals of hard rhombs interdigitate along the twinning line; this interdigitation causes a transverse offset between the twinned crystals and only slightly decreases the entropy of twinned crystals compared to a pure single crystal. In 2D twinned RB crystals, not only is the lattice a mirror image across the twinning line, but the director (i.e., pointing axis) of the rhombs within the lattice is also mirror symmetric.

Interestingly, the observed angle of the RB lattice, which appears just above the transition from hexagonal rotator crystal to RB crystal is much closer to, but slightly below, 90° for rhombs, and this angle is predicted by a rhomboid cage model to increase toward 108° as ϕ_A approaches unity. Also, at lower ϕ_A, the lower symmetry and higher aspect ratio of rhombs, as compared to squares, favor the formation of an interesting variant of a hexatic liquid crystal phase[30,31] between the isotropic and the hexagonal rotator phases.

RESULTS

The progression of observed 2D phases of 72° rhomb colloids for increasing ϕ_A is shown in Figure 1: A spatially and orientationally isotropic phase (I) at low ϕ_A gives way to a hexatic liquid crystal phase[31,32] (H) that has a classic appearance of six azimuthally smeared spots (i.e. a six-fold modulation) in reciprocal space at $\phi_A \approx 0.56$ (Figure 1a). There is a gradual change in bond orientational order from I ($\phi_A \leq 0.54$) to H ($0.54 < \phi_A < 0.565$) that indicates this transition is closer to second order for anisotropic rhombs (see Figure S1b), rather than the first-order transition that is predicted by a simulation for isotropic hard disks.[33] This smearing is reduced substantially at slightly higher $\phi_A \approx 0.57$, yielding a narrow region $0.565 < \phi_A < 0.59$ in which a hexagonal rotator (RX) crystal is found (Figure 1b); this is followed by a crystal−crystal coexistence region (CE) $0.59 \leq \phi_A < 0.60$ (Figure 1c) between highly defected, small domain RX and RB crystals. The CE region is followed by a pure RB phase for $\phi_A \geq 0.60$ (Figure 1d) that can exhibit several forms of twinning and may contain isolated orientational defects. The upper limit of ϕ_A in the RB region is set by a number of factors that influence the maximum applied osmotic pressure in the equilibrated column, including the tilt angle of the sample cell and the total quantity of rhomb particles in the cell.

Because the diameter D of the circle that circumscribes a rhomb is larger than the circumscribed diameter for a square having the same area, the particle densities associated with phase transitions for rhombs occur at smaller ϕ_A than for squares.[25] Also there is a greater spread of center-to-center positions of the rhombs (which can point in different directions) relative to the ideal hexagonal lattice, so the peaks in reciprocal space are smaller and broader for RX of rhombs than for RX of squares (Figure 1b, inset). Intermixing of small crystallites of RX and RB in CE can lead to what effectively appears as hexatic-like features (Figure 1c, inset), but this does not have the same physical origin as the six-fold modulation in the fast Fourier transform (FFT) of the H phase at lower ϕ_A. In the RB phase (Figure 1d), the rhombs tend to point with an average headless director that lies in between the two unit vectors that describe the RB lattice. Interestingly, various forms of twinning of the RB phase are also observed, and we focus on this effect in more detail below.

In Figure 2a, we present measurements of the angle α characterizing the lattice of RX and RB phases (see inset for definition), obtained from average Fourier transforms of images, as a function of ϕ_A. In the RX phase, the lattice angle is $\alpha = 60°$ as expected for a hexagonal lattice. However, for the pure RB phase, just above the coexistence region, we find $\alpha \approx 85°$. Thus, in striking juxtaposition, the RB lattice angle for 72° rhombs is much closer to a square lattice (corresponding to $\alpha = 90°$) than the RB lattice angle for square particles, which have $\alpha \approx 73°$ just above CE.[25] This unexpected behavior is a consequence of rotational entropy and the higher

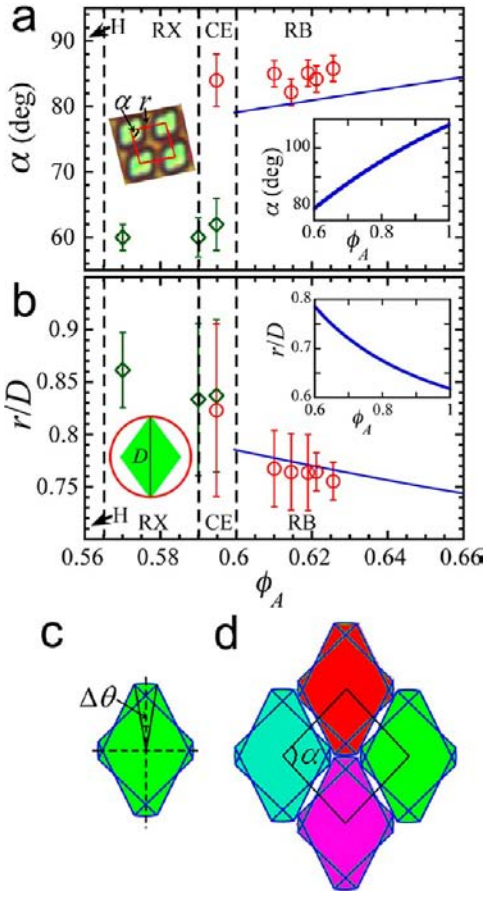

Figure 2. Particle area fraction ϕ_A dependence of the unit cells for observed crystals of Brownian rhombs. (a) Measured lattice angles α (RX, diamonds; RB, circles). Left inset: schematic definitions of α (e.g., for RB) and the center-to-center distance r between rhombs in a unit cell. Right inset: α predicted using the rhomboid model over an extended range of ϕ_A. (b) Measured r normalized by the diameter of a circumscribed circle, D (left inset). Right inset: r/D predicted using the rhomboid model. Solid lines compared with data are rhomboid model predictions. In the CE region, two measured values of α and r/D are shown, corresponding to RX and RB crystallites. (c) Rotating a rhombus about its center $\pm \Delta\theta/2$ sweeps out a rhomboid shape (entire green region). (d) Example of a RB unit cell having angle α formed by packing four rhomboids symmetrically.

aspect ratio and lower symmetry of the rhombs compared to the squares. The dimensionless average center-to-center spacing, r/D, decreases as ϕ_A is raised, as shown in Figure 2b.

A rhomboid model is useful in explaining some of the main features of the observed RB crystals. In Figure 2c, to effectively incorporate rotational entropy into a spatial packing problem, we define a rhomboid shape to be the total swept-out area obtained by rotating a rhombus particle about its center over a range of angles $\pm\Delta\theta/2$. Although an approximation is involved, we effectively convert a complex problem in statistical mechanics of maximizing the combined rotational and translational entropy of hard rhomb particles into a simpler geometrical problem of maximally close-packing rhomboid shapes which cannot overlap. The rhomboid is analogous to the squaroid,[25] and when many rhomboids are packed most efficiently, they undergo a continuous transition from a hexagonal to RB lattice as $\Delta\theta$ decreases (i.e., equivalently as ϕ_A is increased), and the rhomboid's shape changes from disk-like to nearly rhombic. In Figure 2d, we show a symmetric

dx.doi.org/10.1021/ja308214m | J. Am. Chem. Soc. 2012, 134, 18125−18131

packing of four rhomboids that form the unit cell of a RB lattice. The predictions of the rhomboid model for α and r/D are shown as the lines in Figure 2a,b (see Supporting Information for a detailed explanation of the model). Extended predictions of the rhomboid model show a continuous change in $\alpha(\phi_A)$ in the RB phase, and α approaches an angle defined by the particle shape, $180° - 72° = 108°$, as ϕ_A approaches unity and the rhombs fully tile the plane at $r/D = 0.618$. Interestingly, a square phase having $\alpha = 90°$ is predicted to appear only at $\phi_A \approx 0.73$.

A simple contact twin between two entropic RB crystals of hard rhombs is shown in Figure 3a; the contact line (the 2D equivalent of the 3D contact plane), which occurs where the 2D twinned crystals touch, is shown by the dashed line. As in all twinned crystals, the contact line lies along a commonly shared lattice direction of the two twinned crystals where they meet. Due to an entropic preference for interdigitation, which provides an increased number of accessible states to the system of particles, the twinned entropic crystals of hard Brownian particles are shifted along the axis tangent to the contact line by a dimensionless transverse offset $\delta/D \approx 0.3$ (defined as the shorter shift), as shown at $\phi_A = 0.62$.

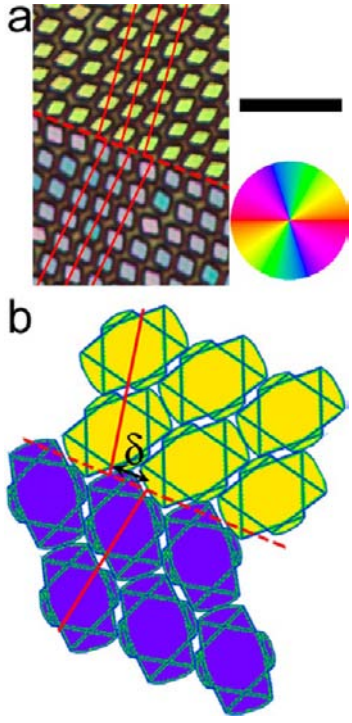

Figure 3. Contact twinning of two RB crystals. (a) Micrograph of observed contact twin ($\phi_A = 0.62$) of RB crystals of rhombs. Color wheel: encodes particle orientations. Red dashed line: mirror line between contact twin crystals, which is parallel to one lattice director of each RB crystal. Red solid lines: the other lattice director of the twin crystals. Scale bar: 10 μm. (b) Idealized rhomboid model of an offset contact twin. The smallest offset distance between the twin lattices along the mirror line is δ.

The fundamental origin of the shift can be inferred from a simple model of rhomboids in a twinned configuration of RB crystals, as shown in Figure 3b. In this figure, $\Delta\theta$ of the rhomboids has been chosen to provide good agreement with both α and r/D of both twinned crystals shown in Figure 3a. The measured transverse offset δ, which arises from interdigitation of the rhomboids along the boundary of the twinned crystals, is apparent in the twinning rhomboid model. Also, in crossing between the two crystals in the contact twin, the average local pointing direction of the rhombs is mirror symmetric. The idealized rhomboid twinning model shows that δ actually depends on ϕ_A and would approach zero continuously as ϕ_A approaches unity.

Upon close inspection and using quantitative image analysis, we find that in a given crystal in the RB phase, on average, there is a slight but measurable deviation of the average director (reflecting the average "molecular" orientation of individual rhombs) from the average bisector of the lattice direction along the diagonal that is closer to the average director of rhombs. We quantify this orientational deviation by γ (see Figure 4 insets for a graphical definition). In Figure 4a,b, we show examples of two different grains of RB crystal that have dominantly left (orange) and right pointing (blue) symmetry breaking, corresponding to probability distributions $p(\gamma)$ that have peaks $\gamma_{max} < 0$ and $\gamma_{max} > 0$, respectively. The distributions can be fit well using a Gaussian distribution, reflecting thermal fluctuations of the orientations of individual rhombs in cages of neighboring rhombs in the RB crystal. Interestingly, due to the reflection symmetry of the twinned crystals across the mirror

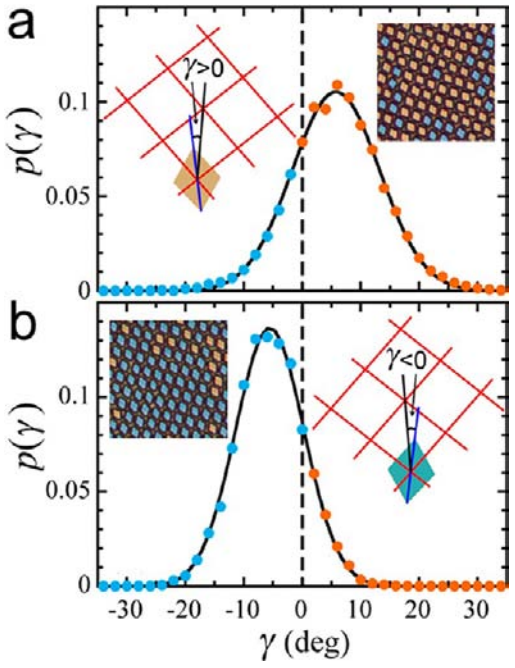

Figure 4. Evidence of chiral symmetry breaking in RB crystals: tilting of rhombs. Time- and ensemble-averaged normalized probability distribution, $p(\gamma)$ (in deg^{-1}), where γ is the angle difference between the orientation of a rhombus and one diagonal direction of the many-particle RB crystal lattice. If the orientation of the rhombus deviates clockwise from the diagonal lattice direction, then γ is negative (blue points and rhombs); otherwise, γ is positive (orange points and rhombs). Black solid lines: least-squares fits to Gaussian functions. (a) Example of positive-deviation RB crystal having average relative orientation $\gamma_{ave} = +5.77 \pm 0.05$ with standard deviation $\gamma_{sd} = 7.47 \pm 0.05$ at $\phi_A = 0.62$. Left inset: schematic showing $\gamma > 0$ for a single rhomb. Right inset: color-coded micrograph that has $\gamma_{ave} > 0$. (b) Example of negative-deviation RB crystal having $\gamma_{ave} = -5.55 \pm 0.04$ with $\gamma_{sd} = 5.83 \pm 0.04$ at $\phi_A = 0.63$. Left inset: color-coded micrograph that has $\gamma_{ave} < 0$. Right inset: schematic showing $\gamma < 0$ for a single rhomb.

dx.doi.org/10.1021/ja308214m | J. Am. Chem. Soc. 2012, 134, 18125−18131

line, one would expect, and our observations also confirm, that these two twinned RB crystals have opposite enantiomeric senses of chiral symmetry breaking (i.e., one has $\gamma_{max} < 0$ and the other has $\gamma_{max} > 0$).

Figure 4 effectively shows a remarkable form of nonlocal chiral symmetry breaking (CSB) that is at least quasi-long range in a crystal phase, since it effectively spans the entire grain until a grain boundary is reached. The longer-range aspect of this chiral symmetry breaking, which is clearly enantiomerically selective within a given grain, distinguishes it from the much shorter-range local chiral symmetry breaking of triangles, which form triatic liquid crystals.[21] The origin of this nonlocal CSB effect is not captured by the simple symmetric rhomboid model of Figure 2d, which emphasizes only rotational degrees of freedom.

We hypothesize that this surprising longer-range CSB effect in RB crystals can arise from a full treatment of a cage model that includes contributions from both translational and rotational degrees of freedom, beyond existing models that consider either only translation[34] or only rotation.[25] In particular, perfect translational alignment of the most pointed vertices of the rhombs is not entropically favored; instead, total entropy maximization favors a slight shift in pointing directions of neighboring rhombs away from the lattice bisector, thereby reducing tip−tip interference. This effectively leads to an average pointing angle γ that is not zero, which is different than the idealized rhomboid model would predict.

In 3D crystals, many different types of twinning, beyond a simple contact twin, can be categorized and identified.[3,4] Among these, we identify two types of structural twins that we commonly observe in 2D RB crystals of 72° rhombs. The first is polysynthetic twinning, a subcategory of multiple twinning, characterized by a plurality of contact twins that have parallel mirror axes; the example in Figure 5a at $\phi_A \approx 0.605$ dominantly

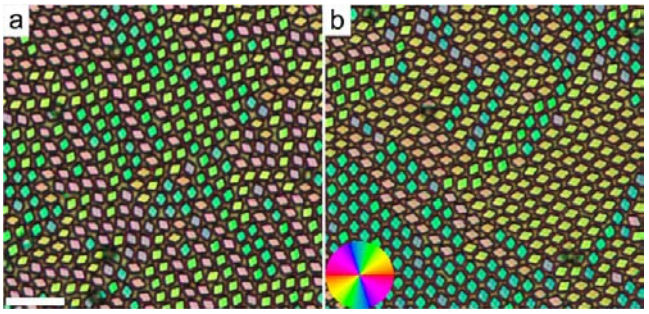

Figure 5. Optical microscopy observations of complex twin structures: (a) Polysynthetic twin ($\phi_A = 0.605$) showing multiple parallel contact mirror lines. (b) Cyclic twin ($\phi_A = 0.615$) showing multiple nonparallel contact mirror lines. Defects cause wandering of the lattice orientations. Scale bar: 10 μm. Color wheel: encodes particle orientations.

shows polysynthetic twinning. The parallel mirror axes tend to give a stripe-like appearance in 2D, similar to striations that are observed on the surfaces of 3D polysynthetic twinned crystals.[1] There are also some defects present that cause the stripes to be limited in length and to wander. The second is cyclic twinning, characterized by a plurality of contact twins that have nonparallel axes; the example in Figure 5b at $\phi_A \approx 0.615$ dominantly shows cyclic twinning in 2D. Due to the symmetry of the RB crystal, there are two equivalent nonparallel axes in the plane along which a twinning line may develop to form a contact twin. Since these twinning lines are not parallel, it is possible to develop cyclic twinning. The nonparallel axes characteristic of cyclic RB twins in 2D can intersect, yielding the appearance of corners in these crystals.

As ϕ_A is increased from RX to RB, the most likely type of identification of twinning in terms of formation is the annealing twin, which can occur in atomic systems as temperature is changed. As in glassy systems that have quenched-in structural disorder, the twinning structures become locked-in (i.e., effectively jammed) after ϕ_A is increased, so further annealing of either polysynthetic or cyclic twins into a larger single crystal is effectively inhibited over reasonably accessible experimental time scales.

In Figure 6, we show examples of isolated defects in RB crystals. A simple point defect consists of a rhomb pointing

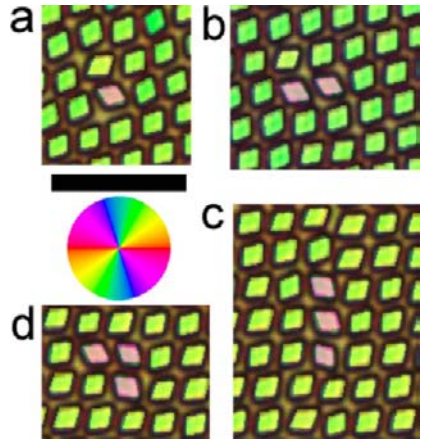

Figure 6. Examples of defects in RB crystals of rhombs. (a) Point defect of a single rhomb having an orientation perpendicular to the preferred orientation of rhombs in the surrounding lattice ($\phi_A = 0.62$). (b) Linear line defect of two rhombs having contrary orientations ($\phi_A = 0.62$). (c) Linear line defect of three rhombs having contrary orientations ($\phi_A = 0.61$). (d) Orthogonal line defect of three rhombs ($\phi_A = 0.61$). Defects create local distortions in the RB lattice. Scale bar: 10 μm. Color wheel: encodes particle orientations.

approximately perpendicular to the other neighboring rhombs in the lattice (Figure 6a). This defect causes a slight deformation of the RB lattice and can cause significant disturbances in the pointing axes of nearest neighboring particles. A point defect can disappear if a large enough local collective density fluctuation occurs such that the cage around the defect dilates, enabling thermal excitations to rotate the trapped particle so that it points along the director. Defects are not entropically favored because they limit the number of accessible positional and orientational configurations of the particles (i.e. both the mis-oriented particle as well as neighboring particles around it). Linear two- and three-particle defects are also seen (Figure 6b,c); defects that contain multiple neighboring rhombs, which all point along the same direction within the defect, appear to be entropically favored over many isolated single-particle defects. By analogy to defect interactions in liquid crystals,[35] one could potentially create an effective attractive potential energy between defects, which is really entropic in origin, to describe the interactions between and clustering of defects, primarily during nucleation and growth. Orthogonal line defects containing three rhombs are also found (Figure 6d). Other larger defects having an even greater number of particles can also be seen in some crystals of the RB

phase. It appears that the defects are quenched-in and that any time for annealing away such point defects is very long, typically beyond an observation time of many hours.

Based on our video particle tracking microscopy (VPTM) analysis of movies, we have also calculated a comprehensive set of structural and orientational order parameters and correlation functions[30] of rhombs at different ϕ_A (see Figures S1−S3). Beyond the structural features that have been our primary focus, we have determined the mean square displacements of translation and rotation of particles over a range of ϕ_A, showing the ultimate translational and rotational trapping of particles as ϕ_A is increased into RB (see Figure S4). The observed changes in particle dynamics are thus clearly linked to the structural changes and the overall phase behavior.

DISCUSSION

It is surprising and interesting that the 72° rhomb shape leads to an extended region of hexatic liquid crystal phase, which is more easily identified than for other particle shapes measured in 2D thus far. The lower symmetry and higher anisotropy of the RB particle shape, compared to squares, are responsible for this effect. Moreover, the nature of the I−H transition for rhombs appears to be continuous (i.e., second order), whereas a prediction of the I−H transition for compact isotropic disks[33] is discontinuous (i.e., first order). The different pointing axes of neighboring rhombs in a local region tend to decorrelate the spatial order over a shorter range, since variation in the local pointing directions of individual rhombs causes a larger spread in the distribution of center-to-center spacings between neighboring rhombs. In addition, the fluctuating randomness of pointing directions of the rhombs at lower densities also favors decorrelation of six-fold bond orientational order over shorter range as ϕ_A is decreased, leading to increased azimuthal smearing of spots in the FFTs. Based on our observations and interpretations, we conjecture that a theoretical model of the I−H transition of Brownian hard rhombs, such as the ones we have studied, will have very different features than the classic theory of the I−H transition for disks. Due to the limited system size over the relevant range of ϕ_A in our experiment, this proposed difference in the order of the I−H transition between hard disks and rhombs, while plausibly revealed by our experiment, requires further confirmation by more extensive experiments and simulations involving many more particles.

Although our detailed study has been limited so far to 72° rhombs, we believe that the basic sequence of phase transitions will be similar, even if the boundary values of ϕ_A differ, as the internal angle characterizing the particles approaches 90°, corresponding to squares. However, in the opposite limit, as the internal angle is reduced further and further, so that the rhombs become more needle-like, we anticipate that the interdigitation between the rhombs will be reduced, and ultimately the H, RX, and RB phases will yield territory to the classic nematic LC phase, known for highly anisotropic rod-like shapes.[36]

As we have pointed out in a prior study of square particle shapes, corner rounding can play a role in the phase behavior and dynamics of the constituent particles.[25,37] Although the rhombs have a minor amount of corner rounding, which arises from the method of fabrication of the particles, we anticipate that rhombs having somewhat lesser degrees of rounding of their corners will exhibit similar phase behavior. However, as the corners of the rhombs become perfectly sharp, predictions of simulations or theory could deviate from what we have observed for rhomb particles that have slight corner rounding.

Many types of simulations, for simplicity, begin with a perfect idealized particle configuration at the very highest particle densities (e.g., in a perfect single crystal using periodic boundary conditions) and relax the system gradually by reducing ϕ_A and re-equilibrating. This is different than our experiments, in which ϕ_A is raised from an isotropic phase through the application of an osmotic pressure and in which twin crystals can grow and imperfections, such as defects, can become trapped. Thus, in order to compare with our experiments, simulations of large systems of hard rhombs would begin in I at low ϕ_A and would raise ϕ_A, thereby providing the potential for statistically predicting formation of various twinning structures, mirror lines, and defects.

Although the rhomboid model can explain many aspects of our observations, it does not explain the observed nonlocal chiral symmetry breaking associated with the pointing directions of rhombs relative to the RB lattice. We believe that this effect can only be explained by a more sophisticated cage model that incorporates local translational as well as rotational motions. Cage models based on rotationally swept particle shapes (which emphasize rotational entropy), such as the rhomboid model, while performing well for a certain limited range of shapes, are not universally applicable and may not perform as well for some other shapes. Thus, our results for rhomb particles show that it would be worthwhile to probe the theoretical limits of applicability of cage models of rotationally swept particle shapes.

It would be interesting to further classify and quantify entropic aspects of defects within the RB crystals. Although we have shown some examples of such defects, there are many questions associated with the effective energetic cost (or, equivalently reduction in entropy) associated with various defects. It is highly likely that the ultimate disappearance of a single orientational defect in an RB crystal will be correlated with local particle density fluctuations; a transient decrease in local density of neighboring particles around a defect may provide enough space for the defected particle to reorient and become a part of the lattice. Further work is required to quantify this coupling and Brownian annealing away of such orientational point defects over time. Likewise, we anticipate that rapid quenching of ϕ_A through the abrupt application of an osmotic pressure (e.g., by using a very high tilt angle of the cuvette in the microscope) will create more highly defected systems and nonequilibrium glassy states.

In entropic twins of rhombs in 2D, there is a slight, yet well-defined translational offset of the mirror-image crystal along the mirror line; this offset arises from entropy maximization. This offset is atypical of atomic twinned crystals made of attractive elements, but offset twinning of hard particles is clearly not parallel growth, a different defect akin to a grain boundary. Parallel growth occurs when neighboring crystals point along the same direction, yet are offset along a line parallel to a lattice vector. In this system of hard rhombs, parallel growth is not observed (or is very rare), since this is entropically unfavorable compared to twinned configurations. However, grain boundaries as well as point and line defects, which are found in many types of colloidal crystals, are also observed in dense RB phases of rhombs, in addition to twinned crystals.

Because there is a small decrease in particle density locally along the twinning line, we anticipate that, if a large enough shear force is applied to one crystal relative to the other along the direction of the twinning line for a simple contact twin, one might observe gliding behavior directly, yielding gliding twins.

However, the interdigitation of the twin crystals along the twinning line over the range of ϕ_A that we observe is strong enough to inhibit gliding, at least from Brownian driving stresses. Alternatively, other forms of non-Brownian forces might cause annealing of defects and enable formation of very large domains of single RB crystals. Overall, the application of non-Brownian driving to systems of rhombs, e.g., arising from externally applied fields, would potentially provide control over these materials, which have interesting tunable optical properties.

CONCLUSION

Concentrated Brownian 2D systems of hard rhombic microparticles have provided the first 2D experimental system of hard colloidal objects in which twinning has been readily observed. Examples of contact, polysynthetic, and cyclic twinned RB crystals have been found. Interdigitation of hard colloidal particles at the contact line in contact twins creates an offset of the crystals that is not typical of twinning of atomic systems in which attractive interactions are important. Twinning may be seen for other types of nonspherical particle shapes in 2D and 3D hard particle systems, and the range of angles of the rhombic particle shape over which twinning is seen, beyond the one example of 72° rhombs that we have shown, still remains as an open question. Beyond crystal twinning, the rhombic particle shape provides an interesting glimpse into a potentially new form of an isotropic−hexatic transition that appears to exhibit significant differences than the classic version of that transition for compact and isotropic disks. The nonlocal form of chiral symmetry breaking within single RB crystals that we observe is not captured by the simplest form of the rhomboid model, so a more sophisticated theoretical approach is needed to explain the relative pointing angle of the particles relative to the RB lattice. Overall, similar to what has been found in other systems of particles having reduced symmetry, such as cylinders and tetrahedra,[38,39] this investigation shows that reducing the symmetry of the particle shape from a square to a rhombus leads to an increase in the richness of observed phase behavior.

ASSOCIATED CONTENT

Supporting Information

Preparation of 2D systems of rhomb particles, quantitative video analysis, Fourier transforms of microscope images, lattice angle and lattice spacing determination, order parameters and correlation functions, measurements of Brownian dynamics, and additional information about the rhomboid model. This information is available free of charge via the Internet at http://pubs.acs.org

AUTHOR INFORMATION

Corresponding Author

mason@chem.ucla.edu

Notes

The authors declare no competing financial interest.

ACKNOWLEDGMENTS

We gratefully acknowledge support from the University of California-Los Angeles.

REFERENCES

(1) Klein, C.; Dutrow, B. *Manual of Mineral Science*, 23rd ed.; Wiley: New York, 2007.
(2) Cahn, R. W. *Adv. Phys.* **1954**, *3*, 363−445.
(3) Klassen-Neklëïudova, M. V. *Mechanical Twinning of Crystals*; Consultants Bureau: New York, 1964.
(4) Hahn, T.; Klapper, H. Twinning of Crystals. In *International Tables for Crystallography Vol. D: Physical Properties of Crystals*; Authier, A., Ed.; Kluwer: Dordrecht, The Netherlands, 2003; p 393.
(5) Donnay, G.; Donnay, J. D. H.; Iijima, S. *Acta Crystallogr.* **1977**, *A33*, 622−626.
(6) Yeates, T. O. *Methods Enzymol.* **1997**, *276*, 344−358.
(7) Ackerson, B. J. *J. Rheol.* **1990**, *34*, 553−590.
(8) Monovoukas, Y.; Gast, A. P. *Langmuir* **1991**, *7*, 460−468.
(9) O'Malley, B.; Snook, I. *Phys. Rev. Lett.* **2003**, *90*, 085702.
(10) Hermes, M.; Vermolen, E. C. M.; Leunissen, M. E.; Vossen, D. L. J.; van Oostrum, P. D. J.; Dijkstra, M.; van Blaaderen, A. *Soft Matter* **2011**, *7*, 4623−4628.
(11) Chen, M.; Kim, J.; Liu, J. P.; Fan, H.; Sun, S. *J. Am. Chem. Soc.* **2006**, *128*, 7132−7133.
(12) Talapin, D. V.; Nelson, J. H.; Shevchenko, E. V.; Aloni, S.; Sadtler, B.; Alivisatos, A. P. *Nano Lett.* **2007**, *7*, 2951−2959.
(13) Pusey, P. N.; van Megen, W. *Nature* **1986**, *320*, 340−342.
(14) Pieranski, P.; Strzelecki, L.; Pansu, B. *Phys. Rev. Lett.* **1983**, *50*, 900−903.
(15) Cheng, Z. D.; Russell, W. B.; Chaikin, P. M. *Nature* **1999**, *401*, 893−895.
(16) Crocker, J. C.; Grier, D. G. *J. Colloid Interface Sci.* **1996**, *179*, 298−310.
(17) Sun, S.; Murray, C. B.; Weller, D.; Folks, L.; Moser, A. *Science* **2000**, *287*, 1989−1992.
(18) Dendukurl, D.; Pregibon, D. C.; Collins, J.; Hatton, T. A.; Doyle, P. S. *Nat. Mater.* **2006**, *5*, 365−369.
(19) Hernandez, C. J.; Mason, T. G. *J. Phys. Chem. C* **2007**, *111*, 4477−4480.
(20) Zhao, K.; Mason, T. G. *Phys. Rev. Lett.* **2009**, *103*, 208302.
(21) Zhao, K.; Bruinsma, R.; Mason, T. G. *Nat. Commun.* **2012**, *3*, 801.
(22) Glotzer, S. C.; Solomon, M. J. *Nat. Mater.* **2007**, *6*, 557−562.
(23) Champion, J. A.; Katare, Y. K.; Mitragotri, S. *Proc. Natl. Acad. Sci. U.S.A.* **2007**, *104*, 11901−11904.
(24) Sacanna, S.; Pine, D. J. *Curr. Opin. Colloid Interface Sci.* **2011**, *16*, 96−105.
(25) Zhao, K.; Bruinsma, R.; Mason, T. G. *Proc. Natl. Acad. Sci. U.S.A.* **2011**, *108*, 2684−2687.
(26) Zhao, K.; Mason, T. G. *Phys. Rev. Lett.* **2007**, *99*, 268301.
(27) Zhao, K.; Mason, T. G. *Phys. Rev. Lett.* **2008**, *101*, 148301.
(28) Asakura, S.; Oosawa, F. *J. Chem. Phys.* **1954**, *22*, 1255−1256.
(29) de Gennes, P. G.; Prost, J. *The Physics of Liquid Crystals*, 2nd ed.; Oxford University Press: Oxford, U.K., 1995.
(30) Chaikin, P. M.; Lubensky, T. C. *Principles of Condensed Matter Physics*; Cambridge University Press: Cambridge, U.K., 1995.
(31) Halperin, B. I.; Nelson, D. R. *Phys. Rev. Lett.* **1978**, *41*, 121−124.
(32) Murray, C. A.; Winkle, D. H. V. *Phys. Rev. Lett.* **1987**, *58*, 1200−1203.
(33) Bernard, E. P.; Krauth, W. *Phys. Rev. Lett.* **2011**, *107*, 155704.
(34) Buehler, R. J.; Wentorf, R. H.; Hirschfelder, J. O.; Curtiss, C. F. *J. Chem. Phys.* **1951**, *19*, 61−71.
(35) Lavrentovich, O. D.; Pasini, P.; Zannoni, C.; Zumer, S. *Defects in Liquid Crystals: Computer Simulations, Theory, and Experiments*; Kluwer: Dordrecht, The Netherlands, 2001.
(36) Onsager, L. *Ann. N.Y. Acad. Sci.* **1949**, *51*, 627−659.
(37) Avendano, C.; Escobedo, F. A. *Soft Matter* **2012**, *8*, 4675−4681.
(38) Li, L.-S.; Walda, J.; Manna, L.; Alivisatos, A. P. *Nano Lett.* **2002**, *2*, 557−560.
(39) Haji-Akbari, A.; Engel, M.; Glotzer, S. C. *J. Chem. Phys.* **2011**, *135*, 194101.